Accurate Heartbeat Detection on Ballistocardiogram Accelerometric Traces

Niccolò Mora, Federico Cocconcelli, Guido Matrella, *Member, IEEE*, and Paolo Ciampolini

***Abstract*— This article presents an automated procedure for acquisition and analysis of BallistoCardioGraphy (BCG) traces. A triaxial accelerometer and a microcontroller unit are used to record heart-induced recoil forces generated from a lying subject. The problem of BCG J-peak annotation is split into two subtasks: candidates extraction, based on a detection signal, and actual annotation, guided by subject-specific search windows. Such a procedure is derived from an automatic calibration, which is carried out with no need of concurrent ElectroCardioGram (ECG) or user intervention. The algorithm also implements postannotation checks for refinement of annotation, which effectively reduces the number of missed J-peaks. The impact of each algorithm phase is analyzed, assessing statistical significance of each step; finally, performance is optimized in a data-driven fashion. Results show that the proposed methodology is able to achieve high sensitivity and precision (the median score is 98.9% and 98.1%, respectively) in J-peak detection. The quality of J-peaks timing annotation is further demonstrated by a very low discrepancy between BCG and ECG heart rate (HR) estimates. Overall population, the standard deviation of such error was found to be approximately 6.56 ms, whereas the mean absolute error was just 4.7 ms (i.e., ≈ 1.18; T_s, where $T_s = 4$ ms is the sampling period). Such scores, indeed, improve over recent related literature.**

***Index Terms*— Accelerometer, Active Assisted Living (AAL), BallistoCardioGram (BCG), heart rate (HR), MEMS, vital signs monitoring.**

I. Introduction

POPULATION aging is seriously challenging sustainability of social and healthcare systems. [1]. Research addressing this scenario increasingly exploits modern information and communication technologies (ICTs). Active and Ambient Assisted Living (AAL; [2], [3]) systems emerged, aiming at making home environments more intelligent and promoting a sustainable model for independent living. For example, an AAL system can help in making services more accessible, by compensating physical or sensory impairments with new smart devices: voice control or even brain–computer interfaces have been introduced to allow severely motor-impaired users to achieve communication and home control [4], [5], exploiting low-cost and easily deployable solutions [6], [7]. Within the realm of smart homes, smart monitoring features can be introduced, exploiting behavioral tracking; for example, machine learning and deep learning techniques have been applied to analyze data collected by home motion sensors [8], [9], highlighting (multivariate) users' patterns and detecting significant behavioral changes over time. AAL monitoring capabilities can be further enhanced by gathering and merging continuous information coming from diverse sources. In particular, fusing behavioral and physiological monitoring could be of great interest, providing a quite comprehensive picture of health and wellbeing status.

Many wearable devices hit the consumer market recently, allowing to monitor physiological parameters. In particular, embedded and low-power technologies allow acquiring information on various vital signs in a noninvasive and minimally obtrusive fashion. For example, heart rate (HR) information can be easily acquired by means of PhotoPlethysmoGraphy (PPG) from wrist-worn devices, which also simultaneously allow acquiring motion data. Recent improvements in Microelectromechanical systems (MEMS) accelerometers or inertial measurement units (IMUs) also made it possible to directly acquire information on heart activity by recording heart-induced vibrational patterns. Interestingly, such patterns can even be extracted by means of noncontact setups, i.e., not requiring the user to carry any wearable device. By using BallistoCardioGraphy (BCG) techniques, an accelerometer can measure heart activity in an indirect fashion, through vibration transmitted from the subject's body to another object (e.g., bed, chair, and body-weight scale), thus resulting in a truly nonintrusive approach. While many BCG implementations reported in the literature [10] exploit piezoelectric sensors placed under the subject, a MEMS accelerometer is used in this article, which allows for a more flexible and unobtrusive setup (in terms of device size and robustness to prolonged use). Accelerometric traces need to be processed, in order to extract parameters of interest; this article presents a methodology for automatic beat annotation on BCG waveforms originated from a person in lying position (i.e., in bed) and measured at the bed itself.

The approach minimizes the need for user intervention; all the procedures, from calibration to data analysis, are carried out in a fully automated fashion, without the need of a concurrent ElectroCardioGram (ECG). Indeed, ECG was acquired here just for performance assessment purposes; comparison with such gold standard shows that very good results can be achieved by the proposed approach, both in terms of heartbeat detection rate and time resolution of beat-to-beat

Manuscript received December 27, 2019; revised April 6, 2020; accepted May 20, 2020. Date of publication May 29, 2020; date of current version October 9, 2020. The Associate Editor coordinating the review process was Sabrina Grassini. *(Corresponding author: Niccolò Mora.)*

The authors are with the Dipartimento di Ingegneria e Architettura, Università degli Studi di Parma, 43124 Parma, Italy (e-mail: niccolo.mora@unipr.it; federico.cocconcelli@unipr.it; guido.matrella@unipr.it; paolo.ciampolini@unipr.it).

Color versions of one or more of the figures in this article are available online at http://ieeexplore.ieee.org.

Digital Object Identifier 10.1109/TIM.2020.2998644

intervals. Also, a preliminary experiment was carried out in an unconstrained, overnight domestic environment to check for more demanding use cases. Although limited in scope, such test matches good quality expectations and allows for looking forward to future solutions, envisaging sensor embedding into smart beds. This would allow to simultaneously acquire information on sleep patterns (duration, times, and quality) and vital signs [e.g., HR and heart rate variability (HRV)], providing relevant insights to health and wellbeing assessment with an inexpensive and minimally intrusive setup.

This article is organized as follows. Section II reviews the related literature and introduces the proposed methodology, including the experimental protocol and details about the implementation of BCG annotation algorithm. Section III presents the results, evaluating the impact of each step of the annotation algorithm on the overall performance, allowing for data-driven optimization. Also, the overall performance metrics are compared to relevant literature works. Finally, Section IV draws the conclusions.

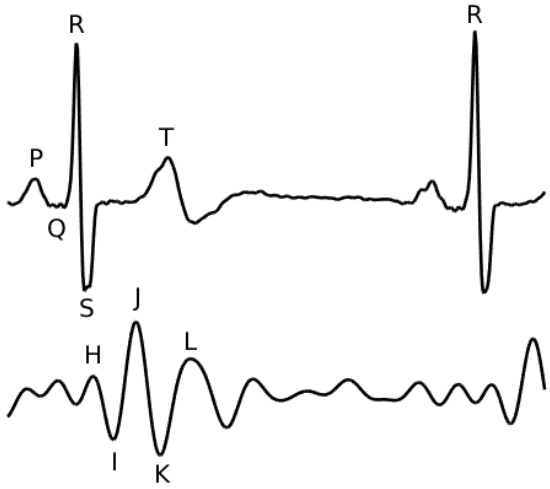

Fig. 1. Correlation between ECG and BCG waveforms.

II. Methods

A. Related Works

Many alternative techniques to ECG exist, aimed at monitoring heart activity in a less intrusive fashion. Although similar in their goal, such techniques exploit a variety of different approaches. SeismoCardioGraphy (SCG) relies on the study of chest vibrations induced by cardiac activity; usually, such vibrations are measured by means of an accelerometer (or IMU) worn at the chest, close to the subject's sternum. SCG signal allows to appreciate many different features of the cardiac mechanical activity [11]. For example, Mora *et al.* [12] presented a fully automated methodology to extract and annotate systolic peaks in SCG; Khosrow-Khavar *et al.* [13] compared four different methods to compute signal envelopes for feature points detection; Choudhary *et al.* [14] exploited wavelet decomposition and reconstruction for identify aortic valve opening (AO) events. Once annotated, such fiducial points can be used for different purposes; for instance, Shandhi *et al.* [15] proposed a regression framework to estimate preejection period (PEP) times for each beat. SCG is exploited for atrial fibrillation detection in [16]. SCG can also act as a proximal reference for pulse transit time calculation [17], in lieu of ECG, enabling cuff-less blood pressure estimate [18], i.e., without requiring oscillometric measurements [19], [20]. Sharing the same principle of SCG, GyroCardioGraphy (GCG) aims at acquiring heart-induced vibration patterns by means of a gyroscope, allowing for better detection of selected features [21]. On a completely different base, HR was estimated on clothed skin in [22] by using an airborne pulse-Doppler ultrasound system; other works use radar systems tuned at different frequency bands [23], [24], laser-Doppler vibrometry [25], [26], microwave sensors [27], and video-based analysis [28].

BCG, on the other hand, studies the whole-body vibrations resulting from recoil forces caused by blood being pumped from the heart. A typical BCG pattern (BCG) is shown in Fig. 1 compared with a coherent (i.e., simultaneously sampled) ECG. The BCG waveform, involving whole-body vibrations, is more related to overall cardiovascular function rather than referring to heart mechanical events (such as SCG and GCG). Therefore, some modeling is needed to correlate BCG acceleration patterns to cardiovascular function phases, accounting for a wider picture including, besides the heart, the whole systemic, and cerebral and pulmonary circulation apparatuses [29]. Techniques for the acquisition of recoil acceleration patterns include load cells or force plates, piezoelectric sensors, and accelerometers. BCG is typically monitored in resting conditions, e.g., in a lying, seated, or standing still posture and efforts are being made to embed BCG measurement devices within familiar, domestic objects, such as chairs, beds, and body-weight scales, in order to reduce intrusiveness as much as possible.

In [30], for instance, modified home weighing scales have been used to acquire BCG vibrations, comparing waveforms acquired with different postures, characterizing the influence of posture on most salient BCG-derived features. In [31], force plates have been used to extract BCG, correlating force-plates peculiar waveform features with those extracted by a weight-scale-based setup. Artifacts introduced by breathing activity were investigated in [32], exploiting piezoelectric thin foils placed under a lying subject and introducing analysis techniques suitable for separating cardiac and respiratory components. Similarly, piezoelectric sensors were exploited for simplified real-time HR measurements [33], [34], detection of atrial fibrillation [35], and nightlong HR monitoring [36]. A slightly different approach consists in measuring BCG by means of an accelerometer attached to the bed frame; such solution, although possibly offering advantages in terms of compactness and robustness of the sensing element, is, indeed, less explored in the literature, where piezoelectric sensors are still more diffused. A clinical trial was conducted in [37], validating a commercial accelerometer-based BCG device by Murata Electronics [38]; on average, the accuracy for HR measurements was found to be -0.5 ± 1.6 beats per minute (mean $\pm$ standard deviation, i.e., -8.3 ± 26.7 ms), with a 97% declared coefficient of determination (R^2) between

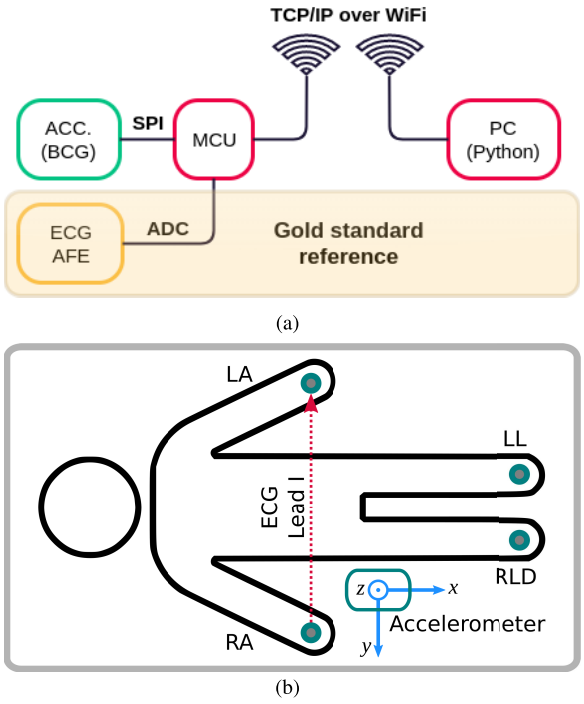

Fig. 2. (a) Acquisition architecture. (b) Measurement setup, with BCG accelerometer and ECG-based validation.

the ECG- and the BCG-based average HR. In this article, we exploit a MEMS accelerometer for BCG traces measurement as well and propose a novel methodology for annotation and calibration, providing high detection sensitivity and precision scores, with very accurate heartbeats interval estimates, also improving over different sensing techniques.

B. Measurement Protocol and Data Acquisition

The BCG acquisition architecture is shown in Fig. 2(a) and consists of four main units.

1) A MEMS accelerometer (Analog Devices ADXL355), which is enclosed in a plastic container (to ensure electrical insulation) and firmly taped below the lying surface (e.g., the bed), in order to guarantee a stable mechanical coupling with the longitudinal recoil forces. In this article, the longitudinal axis, parallel to the head–toe direction, is monitored. The 20-bit ADC conversion of the BCG signal is carried out on board, with a full scale of $\pm 2g$, where g is the acceleration of gravity; the accelerometer's reported noise density is as low as $20\,\mu g/\sqrt{\text{Hz}}$, which is integrated over a passband of ODR/4, where ODR is the output data rate, set at 250 Hz.
2) An ECG recorder, synchronized to the accelerometer rate, allowing to simultaneously record ballistocardiogram and electrocardiogram and thus enabling validation and performance assessment. In particular, a single-lead ECG (lead I) scheme was adopted using disposable Ag/AgCl electrodes. Analog amplification and filtering of the ECG signal were performed by means of the Analog Devices AD8232 front-end device, which was also set to drive the driven right leg DRL) electrode for common-mode noise reduction. Digitalization of the amplified ECG signal is carried out at 12 bits. This is more than sufficient for our purposes, limited to the accurate recording of QRS complexes, to provide ground truth in beat-to-beat interval assessment.
3) A microcontroller unit (MCU) (ARM Cortex M0+) for data synchronization and streaming.
4) A personal computer, which receives and stores data for subsequent (offline) processing.

Sixteen healthy volunteers (6 females and 10 males, min, average, and max age 22, 30.2, and 65, respectively), without any documented history of cardiac pathologies, joined the proposed study, which was conducted following the guidelines of the Helsinki declaration on ethical principles. Each subject was comfortably lying in a supine position during measurements. Recordings lasted 5 min, during which BCG and ECG were acquired simultaneously. The overall measurement setup is shown in Fig. 2(b), which also illustrates the accelerometer reference system.

In order to guarantee a precise phase relationship, both ECG and BCG were synchronously sampled at 250 Hz under MCU control. Data are then transmitted from the MCU over a Wi-Fi network (IEEE 802.11 b/g/n) with the TCP/IP protocol. From the PC receiver side, a Python script allows real-time acquisition and storage of the sampled signals, as well as providing the tools for offline data analysis. Preprocessing is applied to both BCG and ECG waveforms using zero-phase digital filtering techniques in order to maintain the correct phase relationship between them, necessary for accurately assessing the performance of the proposed method. In particular, ECG signals are bandpass filtered by means of a finite impulse response (FIR) filter with a [0.5 Hz, 30 Hz] passband range, whereas a range of [2 Hz, 14 Hz] is used for BCG signals; in both cases, filter order is set to 1024, with filter coefficients computed with the Parks–McClellan algorithm. Individual data are normalized by means of z-scoring: $x_z = (x - \mu_x)/\sigma_x$, where x is the signal of interest, μ_x is its mean, and σ_x is its standard deviation. Finally, in order to extract precise reference systolic time intervals, R-peaks are detected from the ECG gold standard by means of the well-known Pan–Tompkins algorithm [39] and manually checked to ensure proper labeling.

C. Data Analysis

The data analysis procedure is structured in the two main phases: calibration and annotation. Calibration is required to deal with intersubject differences in BCG signal morphology and to make the performance less sensitive to actual features (amplitude, duration, and peaks). Annotation then performs actual beat detection and identification of waveform features, by first detecting the beats coarse location (using a suitably designed signal) and then detecting the characteristic IJK complex, with reference to Fig. 1. In the following, the main analysis components are described.

1) Beat Detection Signals: With reference to Fig. 1, this phase's goal is to detect the IJK complex in the BCG characteristic waveform, just like that the QRS complex is

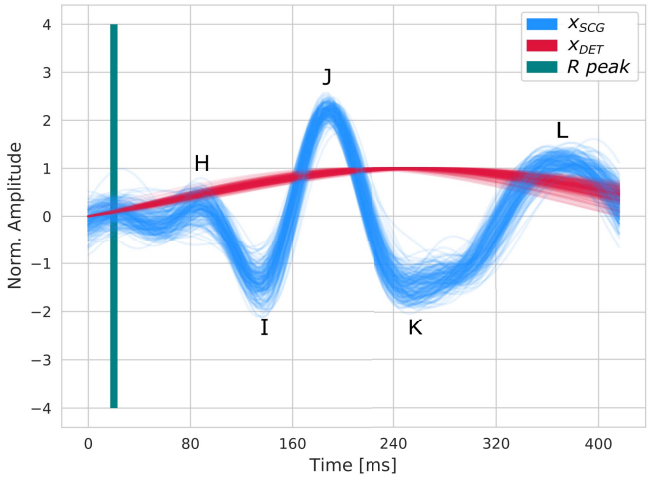

Fig. 3. Ensembles plot of z-scored x_{BCG} signal and min–max scaled x_{DET} signal.

assumed as an ECG periodic feature, suitable for heartbeat detection. However, Fig. 1 shows that the IJK complex is not prominently standing out against the rest of the signal (i.e., it is much less predominant than the QRS complex in the ECG). Hence, the detection signal x_{DET} was introduced, to make such complex more easily discernible

$$x_{\mathrm{DET}}[n] = \sum_{k=0}^{M-1} b[k] \cdot x_{\mathrm{BCG}}^2[n-k] \tag{1}$$

where $x_{\mathrm{BCG}}[n]$ is the bandpass filtered BCG, as described in Section II-B, and $b[k]$ are the coefficients of a low-pass FIR filter ($M = 200$ taps, in this article) with a given cutoff frequency, acting as a smoother (the cutoff frequency is optimized in a data-driven fashion as shown in the results). An example of ensemble plots of x_{BCG} and x_{DET}, obtained from a single subject, is reported in Fig. 3; the reference ECG peak is shown as well, for comparison, together with the annotation of salient BCG points. In order to properly isolate IJK complexes, the resulting x_{DET} signal is further processed by a custom binary filter, considering the sample mean and standard deviation (σ_p) over the last p points ($p = 30$ in this article)

$$x_{\mathrm{SQR}}[i] = \begin{cases} 1, & \text{if } x_{\mathrm{DET}}[i] \geq \mu_{i-p:i} + k \cdot \sigma_{i-p:i} \\ -1, & \text{otherwise} \end{cases} \tag{2}$$

where $\mu_{i-p:i}$ is the sample average over the last p points, σ_{i-p_i} is the sample standard deviations, and k is a multiplication factor that regulates how much the sample needs to be prominent, with respect to the dispersion $\sigma_{i:i-p}$. In this article, k was empirically set to 2, providing a unified reference that was stable across different subjects. By construction, IJK complexes will be located in an interval where x_{SQR} is 1 (positive intervals). Nonetheless, some misdetection may still occur; low-energy beats may still be skipped or neighboring beats can be merged and recognized as a single complex, if the signal energy keeps high enough in between. This results in longer beat intervals than expected; therefore, a second refinement pass is introduced, in which the duration of such candidate intervals is statistically analyzed to detect anomalies: too long positive intervals are split (likely being related to adjacent peaks merging), whereas too long negative intervals are further examined by locally reducing the prominence factor k in. (2), to identify weaker beats. Eventually, validated candidate windows are defined, where J-peaks can be found and annotated, as explained in Section II-C2.

Algorithm 1 Detection of Heartbeat Events

Inputs:

- x_{BCG}: BCG signal

Begin:

- Compute x_{DET} and x_{SQR} [eq. (1) and (2), respectively]
- Find candidate peaks in x_{DET} from x_{SQR}
- ***Calibration***:
  - Validate x_{SQR} positive intervals
  - Find the J peak (maximum in x_{SCG}) within the validated intervals
  - Gather statistics on the difference between x_{DET}'s maximum and the J peak (i.e. the median, $\Delta t_{J,DET}$)
- ***Annotation***:
  - Validate x_{SQR} positive intervals
  - Within those positive intervals, find J peaks at a suitable tolerance distance from x_{DET}'s maximum $t_{DET,i}$ (i.e. s.t. $\left|t_{DET,i} - \Delta t_{J,DET}\right| \leq t_\epsilon$)
  - Mark the corresponding time instant as heartbeat

Return index of possible heartbeats

2) Calibration and Annotation: Intersubject differences complicate the annotation of BCG traces; a calibration phase helps to obtain a subject-adaptive algorithm, suitable for coping with such variations. Basically, a quiet reference period (1 min) is acquired before the actual test waveforms; the beat detection signals described above are computed and candidate beat intervals are extracted, as indicated by the x_{SQR} signal. Then, for each candidate interval, statistics about the distance between the maximum in x_{DET} and the most prominent peak in x_{BCG} are collected. The median value of such distance, $\Delta t_{J,\mathrm{DET}}$, thus allows to estimate where the BCG's J-peak is to be expected with respect to a local maximum in the detection signal; in the annotation mode, such information can be used to coarsely localize J-peaks. In fact, a maximum in x_{BCG}, occurring at time instant $t_{J,i}$, is labeled as J-peak if $|t_{\mathrm{DET},i} - \Delta t_{J,\mathrm{DET}}| \leq t_\epsilon$, where $t_{\mathrm{DET},i}$ is the ith local maximum in x_{DET} (in the ith candidate x_{SQR} epoch) and t_ϵ is a tolerance parameter, which was set to 40 ms in this article. This check ensures a more precise annotation of BCG waveforms, by constraining the search window to given intervals extracted from the more robust x_{DET} and x_{SQR} signals.

To summarize, the calibration and annotation steps are reported as pseudocode in Algorithm 1, whereas Fig. 4 reports the examples of output waveforms from the annotation phase. In Fig. 4 (top), the coherently recorded ECG signal is reported for comparison, with its R-peaks duly annotated for successive performance evaluations. Fig. 4 (center) shows the beat

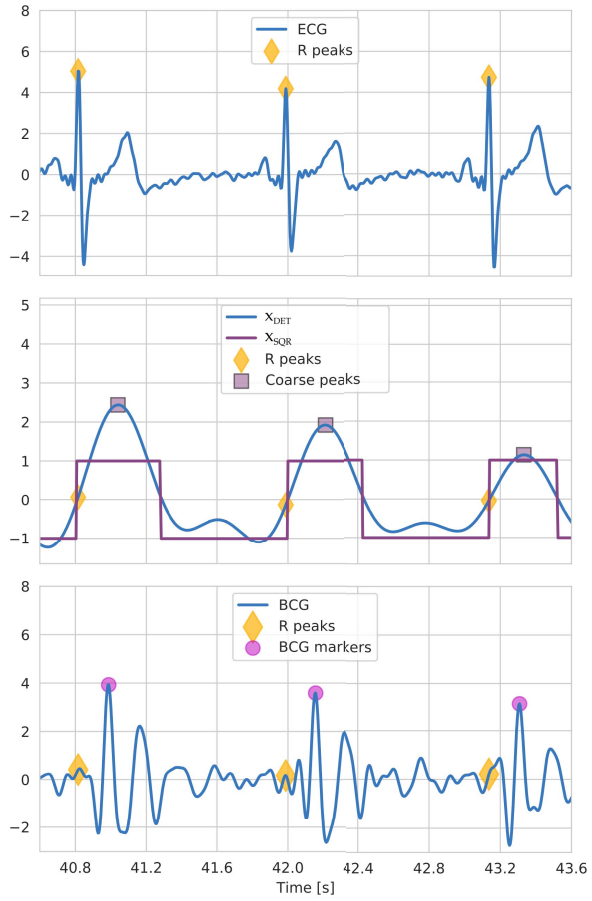

Fig. 4. Top: ECG and R-peaks (yellow diamonds, shown for reference in all panes). Center: beat detector signals, with annotated coarse peaks (purple square). Bottom: BCG signal with annotated peaks.

detection process, with the smooth detection signal x_{DET} and the binarized version x_{SQR}, computed from (2). The intervals where $x_{\mathrm{SQR}} > 0$ are candidates for J-peaks annotation. Fig. 4 (bottom) eventually shows the annotation of the BCG signals in such identified intervals.

III. Results and Discussion

A. Performance Metrics Definitions

The performance characterization of the proposed measurement and processing system targets two aspects as follows.

1) The ability to accurately detect beats, compared with R-peaks ground-truth. In other words, a J-peak should be detected within each R-R interval, with a given tolerance window.
2) The ability to precisely measure beat-to-beat intervals from consecutive J-peaks, with respect to the R-R peaks ground truth. Of course, this definition assumes that the ECG exhibits a regular rhythm, e.g., without ectopic beats. This assumption, indeed, is in line with the intended target population, as better remarked in Section (III-C).

Regarding 1), in order to measure the performance, a target window needs to be defined, relative to each R-peak, where a J-peak should be found. In this article, such window is located between 140 and 260 ms after the R-peak; such a value was found to be adequate for potentially labeling all correct J-peaks, after careful inspection of all waveforms. In more practical terms, a J-peak is correctly detected [true positive (TP)] if one and only one J-peak is found between two R-peaks, within the target window. Peaks detected outside that window are considered false positives (FPs), whereas a missed detection within such time frame is considered to be a false negative (FN). Based on these definitions, we can express the performance metrics of interest as follows.

1) *Sensitivity:* Percentage of correctly identified J-peaks (ECG provides the reference location and beat counts): $\mathrm{Sn} = 100\% \cdot \mathrm{TP}/(\mathrm{TP} + \mathrm{FN})$.
2) *Precision:* Percentage of FP in all detected J-peaks: $\mathrm{Pr} = 100\% \cdot \mathrm{TP}/(\mathrm{TP+FP})$.
3) *F1 Score:* It combines precision and sensitivity into a single indicator (actually, their harmonic mean): $F1 = 100\% \cdot 2 \cdot (\mathrm{Sn} \cdot \mathrm{Pr})/(\mathrm{Sn+Pr})$.

As far as the ability to precisely measure beat-to-beat intervals is concerned (as stated in item 2), the error between the corresponding R-R and J-J intervals was measured as follows:

$$e_i = (t_{R,i} - t_{R,i-1}) - (t_{J,i} - t_{J,i-1}) \tag{3}$$

with $i = (1, \ldots, N_B - 1)$, where N_B is the number of detected beats, e_i is the ith error term, $t_{R,i}$ is the ith R-peak, and $t_{J,i}$ is the ith J-peak. For convenience, we also define e as the time series of errors e_i and t_{RR} and t_{JJ} as the time series of R-R and J-J intervals, respectively. Then, in order to assess the annotation performance, the following metrics were used.

1) The mean error ($\mu_e = E\{e_i\}$), representing the bias between t_{RR} and t_{JJ}.
2) The standard deviation of the error, representing uncertainty: $\sigma_e = (E\{(e_i - \mu_e)^2\})^{1/2}$.
3) The mean absolute error: $\mathrm{MAE} = E\{|e_i|\}$.

B. Performance Assessment

It is convenient to independently assess the impact that each phase of the algorithm has on the overall performance. First, let us examine the performance obtained by separating J-peak detection in two distinct steps (coarse peak localization and annotation) instead of a single-step straightforward BCG-thresholding strategy. In the latter case, the performance is strictly dependent on such a unique threshold; high values increase precision, at the expense of sensitivity (limited by FNs), whereas lowering the threshold improves sensitivity but has a negative impact on precision. In other terms, it is troublesome to achieve a well-balanced tradeoff. By introducing the two-step strategy described earlier, fairly good performance was obtained; on average, the sensitivity was found to be 96.8%, with 97.0% precision (i.e., an F1 score of 0.969), and such results represent the baseline over which successive processing steps should improve.

Let us then assess the performance increase introduced by second-pass refinements during the detection phase. As discussed in Section II-C1, too-long J-J intervals may be detected,

due to either merging of two (or more) adjacent high-energy beats or skipping a low-energy beat. By comparing the current interval with a running estimate of beat-to-beat intervals, lengthened frames can be detected and a search for potentially missing beats can be performed, thereby lowering the k value in (2). In our tests, such a local refinement yielded an increase of the average sensitivity up to 97.9% (i.e., +1.1%). Such improvement, although small in absolute terms, is quite relevant with respect to the available sensitivity margin and is statistically significant indeed; a Wilcoxon signed-rank test over the population scores yields $p \approx 0.01$. Precision is not affected at all, showing that no further FP was introduced. In other words, the refinement procedure was, indeed, able to discover additional true peaks.

The calibration phase was then introduced, aimed at optimally sizing the search window for J-peaks. In fact, it can be observed that the average distance between the J-peaks and the nearest detector signal maximum, $\Delta t_{J,\mathrm{DET}}$, is somehow dispersed among different subjects; such values ranged from 32 up to 124 ms. Accounting for such a large range requires to keep a conservatively large search window, possibly limiting the effectiveness of the coarse peak localization strategy described so far. Subjectwise calibration was therefore introduced, according to the procedure illustrated in Section II-C2, yielding a further increase in both sensitivity (from 97.9% to 98.5%, on average) and precision (from 97.0% to 97.5%); in this case too, such marginal improvements are statistically significant (the difference of individual subject scores in the two conditions was assessed by means of the Wilcoxon signed-rank test, yielding $p \approx 0.03$).

Another parameter that affects performance is the cutoff frequency of the low-pass filter used for smoothing the detection curve, x_{DET}; in fact, setting a too low cutoff frequency causes the signal to vary too slowly, making it difficult to discriminate between the adjacent beats and possibly yielding aggregation of multiple beats. This, in turn, jeopardizes sensitivity due to some actual beats remaining undetected. On the other hand, the higher the cutoff frequency, the closer x_{DET} resembles the squared BCG signal, for which the precision performance degrades (i.e., FPs may be introduced by the x_{DET} curve). In order to optimize both sensitivity and precision, the F1 score was chosen as maximization target; a sensitivity analysis was conducted on the smoother cutoff frequency (f_{LP}), the results of which are shown in Fig. 5. Here, the F1 score over all subjects is represented, as a function of f_{LP}. The shaded area beside the F1 curve represents the interquartile range (IQR, i.e., 25th–75th percentile range). As expected, for very low cutoff frequencies, low values of F1 score are achieved; sensitivity is poor due to many peaks not being detected. On the other hand, for higher frequency values, the F1 metric suffers some limitations due to poorer precision; spurious candidate beats are detected in this case, yielding FPs. By inspection of Fig. 5, it can be noticed that the maximum performance is achieved at $f_{\mathrm{LP}} = 1.8$ Hz (median F1 score is 0.986); nonetheless, a practical range between 1.1 and 2.1 Hz exists, where performance is still comparable (in statistical terms) to the maximum (as pointed out by adjusted the Wilcoxon signed-rank test, with a significance level set to 0.05).

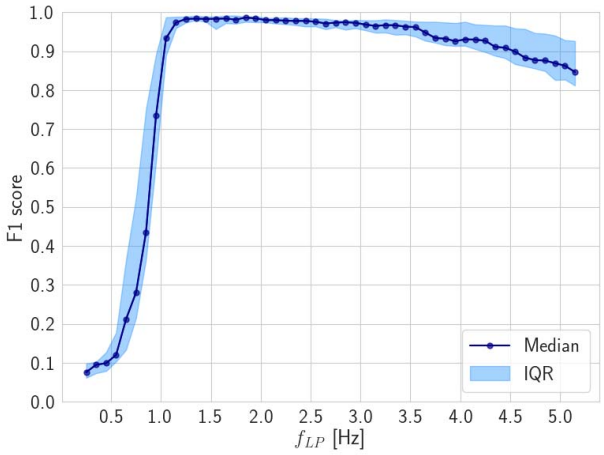

Fig. 5. F1 score as a function of the cutoff frequency: each data point represents the median of subject-individual scores, whereas shaded areas show the 25th–75th percentile range.

C. Overall Performance Discussion

As discussed in Section I, this article focuses on solutions suitable for domestic environments, in a continuous, multidimensional monitoring scenario. Therefore, the tool is not intended as a replacement for clinical instruments. Indeed, the approach is not meant for dealing with heart pathology detection and classification, but, instead, for picking up long-term trends and patterns in a nonobtrusive fashion; the intended targets are senior citizens in relatively good health status, not suffering from major cardiac issues. For this reason, the methods were tested on healthy subjects. Furthermore, since home deployment is envisioned in the future, it is worth remarking that the methodology is carried out in a completely automatic fashion, without requiring significant inputs from the user. Also, the ECG waveforms collected in this study were only used to assess the performance of the proposed methods and were not used to guide the annotation process in any way.

The performance metrics introduced in Section III-A were evaluated on the full data set, aiming at quantifying the detection capability as well as the accuracy in beat interval measurements. As far as the former is concerned, Fig. 6(a) shows the box plots of the sensitivity, precision, and F1 scores: median values of 98.9%, 98.1%, and 98.5% are found, respectively. Such results highlight an overall good detection performance; in absolute terms, on average, only 3.7 heartbeats were missed (over 5 min) for each subject in the data set, with just 5.4 FP events. The evaluated metrics are quite compact, with just a few subjects performing slightly worse than others. For example, subject 4 achieves the lowest sensitivity, precision, and F1 scores (94.7%, 93.5%, and 94.1%, respectively), whereas subject 5 achieves the second lowest scores in precision and F1 (94.1% and 95.1%, respectively); such points are highlighted as potential outliers in Fig. 6(a) (together with subject 7 that scores 95.8% in precision). Nonetheless, such performance values are quite high, considering that no data were previously discarded (e.g., by filtering out segments affected by

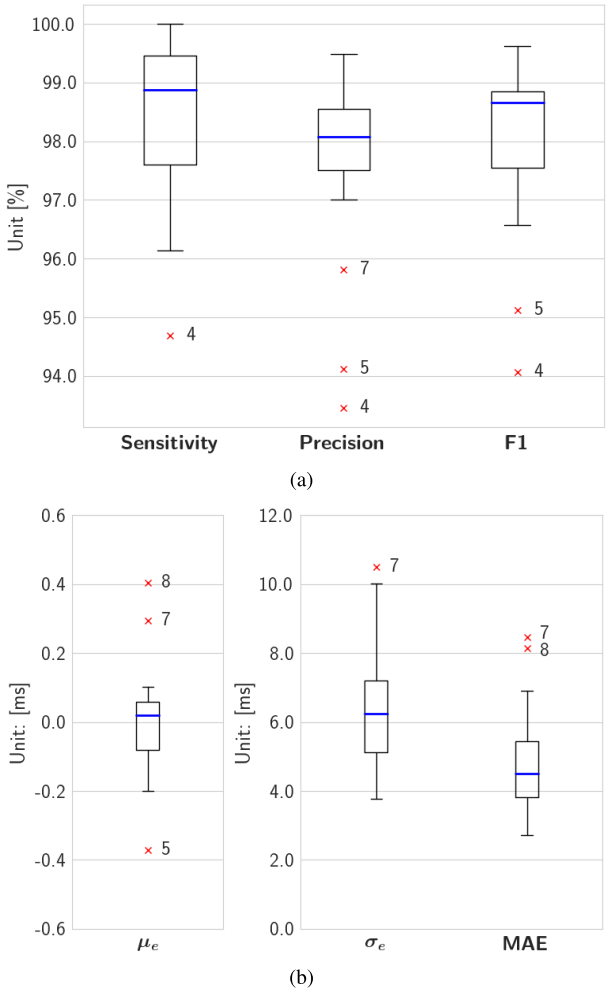

Fig. 6. Box plots of performance metrics. (a) Beat detection. (b) Beat interval measurement. Potential outliers are marked as red crosses, annotated with the subject ID.

slight motion artifacts). In particular, the reported precision is comparable with other works in the literature [32], [36], while better sensitivity performance is obtained (with the best value of 92.7% reported in [32]).

The performance in heartbeat intervals estimation was assessed on all subjects' records. From (3), the error is defined as the difference between the corresponding R-R and J-J intervals. The results of such evaluations are reported in Fig. 6(b) as box plots. In particular, it can be noticed that the median bias between the R-R and J-J measurements, μ_e, is almost null. Just a few potential outliers emerge (subjects 5, 7, and 8). Nonetheless, such values are less than 0.4 ms (in absolute terms) which, in turn, is just a fraction of the sampling period ($T_s = 4$ ms); thus, the bias error μ_e can be practically neglected. Errors' standard deviation (σ_e) achieves a median value of 6.2 ms, with subject 7 emerging as a potential outlier again, as shown in the box plot. However, it is worth noting that if errors in J-peak annotations happen on two consecutive beats (e.g., leading in the first one and lagging in the second), the total error in that J-J interval estimation may appear larger than the others; standard deviations may increase due to larger, although rare errors. Therefore, the MAE was also computed,

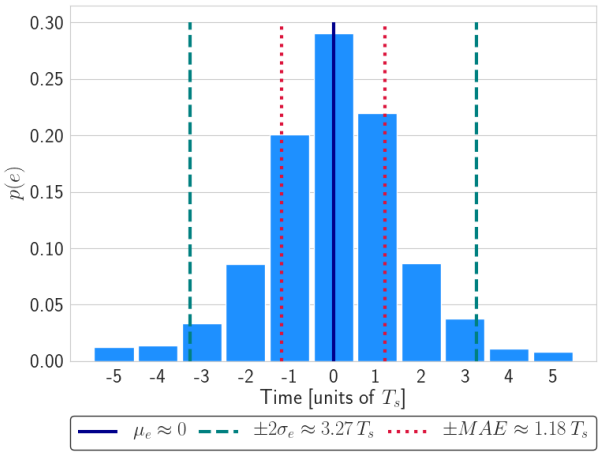

Fig. 7. Histogram of measurement errors between the R-R and J-J intervals, in units of sampling interval T_s.

providing a more stable metric of the error in the beat-to-beat interval estimation. The median score for MAE is 4.5 ms, with subjects 7 and 8 slightly above the others; at the same time, however, such subjects exhibit the larger mean beat-to-beat intervals and the larger HRV (defined as the standard deviation of the difference between consecutive heartbeat intervals): the relative impact of such measurement errors is, therefore, more contained.

By considering the full records as a unique population, Fig. 7 shows a histogram approximation of the beat-to-beat interval measurement errors. On average, the bias between the R-R and J-J intervals is still approximately null ($\mu_e \approx 0$), indicating good mean agreement. Errors' standard deviation σ_e and MAE are approximately 1.64 T_s (6.56 ms) and 1.18 T_s (4.7 ms), respectively. Such errors are small compared with the average heartbeat interval observed ($\approx$ 1045.6 ms); also, the MAE is just 7% of the average HRV.

A different visualization of error distribution is shown in the Bland–Altman plot of Fig. 8; on the x-axis, the average of R-R and J-J interval measurements is reported, whereas the y-axis shows their difference. The σ_e and MAE metrics achieved by the proposed method favorably compare with other works in the literature. For example, Paalasmaa *et al.* [36] compared different setups in terms of sex, single/double bed, and sensor type. In particular, for single bed, an MAE of 13.22 ms is achieved (at a sample frequency of 300 Hz, i.e., $T_s = 3.33$ ms); however, no statistically significant difference is found between those factors. On the other hand, Alvarado-Serrano *et al.* [40] reports a standard deviation $\sigma_e = 14.35$ ms; a similar setup, featuring a commercial, accelerometer-based solution [37], achieved -0.5 ± 1.6 beats per minute (mean $\pm$ standard deviation, i.e., -8.3 ± 26.7 ms) in HR estimation accuracy. Finally, the degree of agreement between t_{RR} and t_{JJ} can be evaluated by means of the coefficient of determination (R^2). As shown in Fig. 9, there is a very high agreement between the two measurements, with $R^2 = 99.8\%$ scored over the full data set. This, again, favorably compares with the similar setup in [38], where an $R^2 = 97\%$ score is reported.

TABLE I

COMPARISON OF AVERAGE (ACROSS INDIVIDUAL) SCORES BETWEEN THE EXAMINED DATA SET (DATA SET 1) AND A SIMILAR ONE USING A DIFFERENT BED FRAME (DATA SET 2)

	Sensitivity [%]	**Precision [%]**	**R^2 [%]**	**MAE [ms]**	**RMSE [ms]**
Mean [95% CI]	98.4	97.6	98.8	4.7	6.5
Dataset 1	[97.6-99.2]	[96.7-98.5]	[98.5-99.2]	[3.8-5.8]	[5.4-7.6]
Mean [95% CI]	97.4	97.0	97.9	4.0	5.9
Dataset 2	[95.7-99.1]	[95.4-98.6]	[96.1-99.7]	[2.9-5.2]	[4.4-7.3]
***p-value* (Mann-Whitney U test)**	0.307	0.456	0.439	0.091	0.221

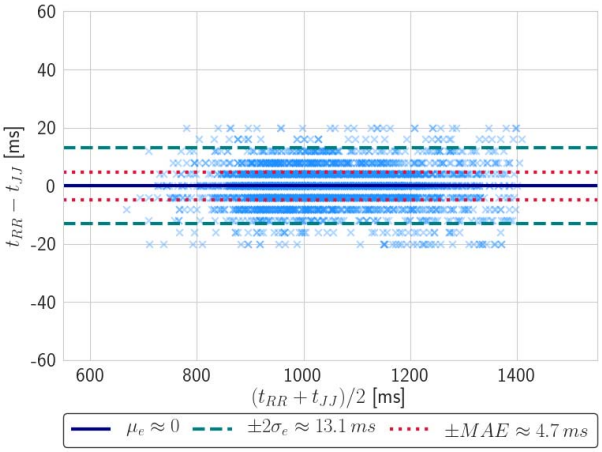

Fig. 8. Bland–Altman plot of full population, detailing the agreement between the R-R and J-J intervals.

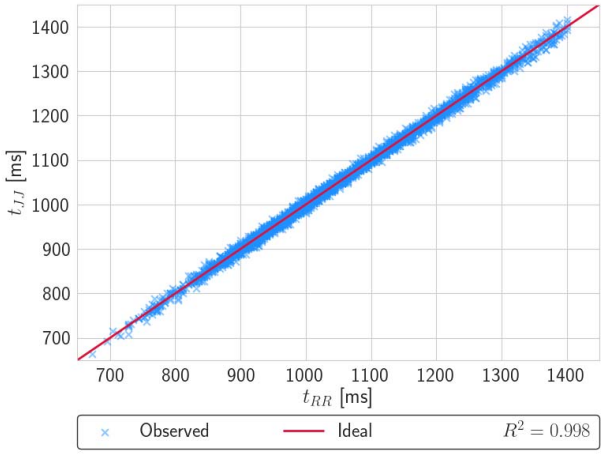

Fig. 9. Correlation plot of full population, detailing the agreement between t_{RR} and t_{JJ}.

A further test was carried out, in order to assess the stability of the proposed methodology. To this purpose, another data set was considered, from now on named Data Set 2 (DS2) [while the previous one will be referred to as Data Set 1 (DS1)]. DS2 comes from a different study, mostly aimed at evaluating acceptability and performance in a realistic deployment situation. For the sake of conciseness, we shall omit the detailed discussion of performance metrics (as given already for DS1) in this case. We shall limit ourselves to mention the only differences in experimental setup between the two data sets, which are listed in the following.

1) *Sampling Rate:* For DS1, it was set to 250 Hz, whereas DS2 was acquired at 500 Hz.
2) *Accelerometer Placement:* To obtain DS2, a commercial bed and mattress was used. The sensor was firmly attached to a bed slat under the mattress, below the chest. This allows testing a setting much closer to target deployment, where installation needs to be as minimally obtrusive as possible.

Fourteen subjects (5 females and 9 males, min, average, and max age 22, 28.1, and 46 years, respectively, not included in DS1 population) were recruited for DS2, according to the same guidelines and setup. The very same methodology described earlier was applied to DS2, with no modifications. Table I reports the achieved performance, in terms of individual scores averages; for comparison's convenience, the metrics relative to DS1 are also recalled. In order to assess whether the scores differ significantly between data sets, a Mann–Whitney U-test was carried out on the two populations of individual scores. The associated p-value is reported in Table I as well. In particular, it can be noticed that the performance scores achieved in terms of beat detection are comparable, with no statistical difference between data sets at a significance level of 0.05. Furthermore, no significant evidence of annotation error improvement is gathered (in terms of MAE and RMSE), thus suggesting that the scores achieved on DS1 are not particularly impacted by the lower temporal resolution. Such observation is important if an embedded implementation is envisaged; in this case, power consumption can be optimized by running at lower speed.

As a final remark, it is worth mentioning that both data sets were acquired in lab-controlled conditions, with subjects lying on the same bed structure. Although different beds were used in DS1 and DS2, such potential limitation is being addressed (on a wider bed features range) by ongoing investigations on long-term, unconstrained home scenarios. Nevertheless, encouraging results come from preliminary results of such investigation: data obtained from one subject, recorded for approximately 6 h during night sleep, are in line with the lab results. Approximately, just 2% of the data was discarded, due to motion artifacts corrupting the ECG (i.e., the ground truth) and thus making validation of BCG (although acquired) impossible. On the valid set, a 95.4% sensitivity was achieved, with a 94.8% precision; on the other hand, heartbeat intervals measurement seems improved, featuring an MAE of just 3.54 ms, σ_e of 5.12 ms, and an R^2 score of 99.7%.

Such results support portability of the proposed methodology to real-life context, where long-term, overnight monitoring of HR and HRV is envisioned; in such a scenario, the same sensors might also gather information on unconscious movements, which may contribute to sleep quality assessment and therefore effectively complement higher level behavioral analyses.

IV. Conclusion

This article presented an automated procedure for acquisition and analysis of BCG traces. A MEMS accelerometer was used to record heart-induced recoil forces, generated from a lying subject; simultaneously, for performance assessment purposes, a lead-I ECG was acquired. The BCG waveforms were analyzed in a fully unsupervised way, i.e., without the need for concurrent ECG information to guide signal segmentation and annotation. Instead, such a procedure was implemented in a two-step fashion, by first identifying candidate intervals containing J-peaks and then annotating actual BCG waveforms. An automated calibration procedure was devised, to adapt the methodology to each individual subject. Furthermore, a refinement pass is performed after the first annotation procedure, to recover potentially missing beats by analyzing the detected beat-to-beat time series. The impact of each algorithm phase was rigorously analyzed, justifying each step by assessing its statistical significance; in addition, the final performance was optimized in a data-driven fashion, by selecting optimal filtering options.

The approach features good performance in detecting J-peaks in BCG measured waveforms: by assuming R-peaks in ECG as a reference, a median 98.9% sensitivity and 98.1% precision scores (yielding a 98.7% median F1 score). The time accuracy of BCG annotation was also assessed by comparing the J-J intervals with the gold-standard R-R ones; the results show that a very low error standard deviation ($\sigma_e \approx 6.56$ ms) and MAE (MAE $\approx$ 4.7 ms) are achieved, which improves over literature.

The presented methodology well suits the framework of continuous monitoring; through BCG, basic information about heart activity can be derived [e.g., HR and HRV], in an unobtrusive fashion. Such data may enhance the dimensionality and richness of AAL-oriented analysis. For example, HR and HRV parameters may be fused with information about bed presence and movements, which could be extracted from the very same accelerometer outputs. This would allow for implementing more expressive and detailed sleep analysis. Preliminary tests on unconstrained home scenarios confirm the feasibility of the presented methodology, with precision and sensitivity still standing in the practical range and even improving over the MAE and σ_e scores. This perspectively enables the development of low-cost smart beds fitting the AAL paradigm. More generally speaking, the approach discussed earlier lends itself to implement low-cost and low-intrusiveness estimate of heart parameters and is therefore particularly suitable for enabling basic heart monitoring functionality into further smart home objects, fully matching the Internet-of-Things vision.

Acknowledgment

The authors would like to thank Dr. Riccardo Piazza for his contribution in developing part of the measurement system and for the help in data collection.

References

[1] C. Colombier, "Population ageing in healthcare–a minor issue? Evidence from Switzerland," *Appl. Econ.*, vol. 50, no. 15, pp. 1746–1760, Mar. 2018.

[2] C. Dobre, C. X. Mavromoustakis, N. M. Garcia, G. Mastorakis, and R. I. Goleva, "Introduction to the AAL and ELE systems," in *Ambient Assisted Living and Enhanced Living Environments*. Amsterdam, The Netherlands: Elsevier, 2017, pp. 1–16.

[3] C. Guerra *et al.*, "The HELICOPTER project: A heterogeneous sensor network suitable for behavioral monitoring," in *Ambient Assisted Living. ICT-based Solutions in Real Life Situations* (Lecture Notes in Artificial Intelligence and Lecture Notes in Bioinformatics), vol. 9455. Cham, Switzerland: Springer, 2015, pp. 152–163.

[4] S. Saeedi, R. Chavarriaga, and J. del R. Millán, "Long-term stable control of motor-imagery BCI by a locked-in user through adaptive assistance," *IEEE Trans. Neural Syst. Rehabil. Eng.*, vol. 25, no. 4, pp. 380–391, Apr. 2017.

[5] N. Mora, I. De Munari, P. Ciampolini, and J. R. del Millán, "Plug&play brain–computer interfaces for effective active and assisted living control," *Med. Biol. Eng. Comput.*, vol. 55, no. 8, pp. 1339–1352, Aug. 2017.

[6] N. Mora, I. De Munari, and P. Ciampolini, "Subject-independent, SSVEP-based BCI: Trading off among accuracy, responsiveness and complexity," in *Proc. 7th Int. IEEE/EMBS Conf. Neural Eng. (NER)*, Apr. 2015, pp. 146–149.

[7] N. Mora, I. De Munari, and P. Ciampolini, "Improving BCI usability as HCI in ambient assisted living system control," in *Foundations of Augmented Cognition* (Lecture Notes in Artificial Intelligence and Lecture Notes in Bioinformatics), vol. 9183. Cham, Switzerland: Springer, 2015, pp. 293–303.

[8] N. Mora, G. Matrella, and P. Ciampolini, "Cloud-based behavioral monitoring in smart homes," *Sensors*, vol. 18, no. 6, p. 1951, Jun. 2018.

[9] C. Debes, A. Merentitis, S. Sukhanov, M. Niessen, N. Frangiadakis, and A. Bauer, "Monitoring activities of daily living in smart homes: Understanding human behavior," *IEEE Signal Process. Mag.*, vol. 33, no. 2, pp. 81–94, Mar. 2016.

[10] Z. He *et al.*, "A heart rate measurement system based on ballistocardiogram for smart furniture," in *Proc. IEEE Asia Pacific Conf. Circuits Syst. (APCCAS)*, Oct. 2018, pp. 151–154.

[11] G. Shafiq, S. Tatinati, W. T. Ang, and K. C. Veluvolu, "Automatic identification of systolic time intervals in seismocardiogram," *Sci. Rep.*, vol. 6, no. 1, p. 37524, Dec. 2016.

[12] N. Mora, F. Cocconcelli, G. Matrella, and P. Ciampolini, "Fully automated annotation of seismocardiogram for noninvasive vital sign measurements," *IEEE Trans. Instrum. Meas.*, vol. 69, no. 4, pp. 1241–1250, Apr. 2020.

[13] F. Khosrow-khavar, K. Tavakolian, A. P. Blaber, J. M. Zanetti, R. Fazel-Rezai, and C. Menon, "Automatic annotation of seismocardiogram with high-frequency precordial accelerations," *IEEE J. Biomed. Health Inform.*, vol. 19, no. 4, pp. 1428–1434, Jul. 2015.

[14] T. Choudhary, L. N. Sharma, and M. K. Bhuyan, "Automatic detection of aortic valve opening using seismocardiography in healthy individuals," *IEEE J. Biomed. Health Inform.*, vol. 23, no. 3, pp. 1032–1040, May 2019.

[15] M. M. H. Shandhi, B. Semiz, S. Hersek, N. Goller, F. Ayazi, and O. T. Inan, "Performance analysis of gyroscope and accelerometer sensors for seismocardiography-based wearable pre-ejection period estimation," *IEEE J. Biomed. Health Inform.*, vol. 23, no. 6, pp. 2365–2374, Nov. 2019.

[16] T. Hurnanen *et al.*, "Automated detection of atrial fibrillation based on time–frequency analysis of seismocardiograms," *IEEE J. Biomed. Health Inform.*, vol. 21, no. 5, pp. 1233–1241, Sep. 2017.

[17] C. Yang and N. Tavassolian, "Pulse transit time measurement using seismocardiogram, photoplethysmogram, and acoustic recordings: Evaluation and comparison," *IEEE J. Biomed. Health Inform.*, vol. 22, no. 3, pp. 733–740, May 2018.

[18] A. Esmaili, M. Kachuee, and M. Shabany, "Nonlinear cuffless blood pressure estimation of healthy subjects using pulse transit time and arrival time," *IEEE Trans. Instrum. Meas.*, vol. 66, no. 12, pp. 3299–3308, Dec. 2017.

[19] M. Forouzanfar, S. Ahmad, I. Batkin, H. R. Dajani, V. Z. Groza, and M. Bolic, "Model-based mean arterial pressure estimation using simultaneous electrocardiogram and oscillometric blood pressure measurements," *IEEE Trans. Instrum. Meas.*, vol. 64, no. 9, pp. 2443–2452, Sep. 2015.

[20] K. Barbe, W. Van Moer, and D. Schoors, "Analyzing the Windkessel model as a potential candidate for correcting oscillometric blood-pressure measurements," *IEEE Trans. Instrum. Meas.*, vol. 61, no. 2, pp. 411–418, Feb. 2012.

[21] C. Yang and N. Tavassolian, "Combined seismo- and gyro-cardiography: A more comprehensive evaluation of heart-induced chest vibrations," *IEEE J. Biomed. Health Inform.*, vol. 22, no. 5, pp. 1466–1475, Sep. 2018.

[22] N. Jeger-Madiot, J. Gateau, M. Fink, and R.-K. Ing, "Non-contact and through-clothing measurement of the heart rate using ultrasound vibrocardiography," *Med. Eng. Phys.*, vol. 50, pp. 96–102, Dec. 2017.

[23] S. Kazemi, A. Ghorbani, H. Amindavar, and D. R. Morgan, "Vital-sign extraction using bootstrap-based generalized warblet transform in heart and respiration monitoring radar system," *IEEE Trans. Instrum. Meas.*, vol. 65, no. 2, pp. 255–263, Feb. 2016.

[24] J. Tu and J. Lin, "Fast acquisition of heart rate in noncontact vital sign radar measurement using time-window-variation technique," *IEEE Trans. Instrum. Meas.*, vol. 65, no. 1, pp. 112–122, Jan. 2016.

[25] G. Cosoli, L. Casacanditella, E. P. Tomasini, and L. Scalise, "The non-contact measure of the heart rate variability by laser Doppler vibrometry: Comparison with electrocardiography," *Meas. Sci. Technol.*, vol. 27, no. 6, Jun. 2016, Art. no. 065701.

[26] L. Scalise, V. M. Primiani, P. Russo, A. De Leo, D. Shahu, and G. Cerri, "Wireless sensing for the respiratory activity of human beings: Measurements and wide-band numerical analysis," *Int. J. Antennas Propag.*, vol. 2013, pp. 1–10, Apr. 2013.

[27] G. Lu, F. Yang, Y. Tian, X. Jing, and J. Wang, "Contact-free measurement of heart rate variability via a microwave sensor," *Sensors*, vol. 9, no. 12, pp. 9572–9581, Nov. 2009.

[28] M. Villarroel *et al.*, "Continuous non-contact vital sign monitoring in neonatal intensive care unit," *Healthcare Technol. Lett.*, vol. 1, no. 3, pp. 87–91, Sep. 2014.

[29] G. Guidoboni *et al.*, "Cardiovascular function and ballistocardiogram: A relationship interpreted via mathematical modeling," *IEEE Trans. Biomed. Eng.*, vol. 66, no. 10, pp. 2906–2917, Oct. 2019.

[30] A. Q. Javaid, A. D. Wiens, N. F. Fesmire, M. A. Weitnauer, and O. T. Inan, "Quantifying and reducing posture-dependent distortion in ballistocardiogram measurements," *IEEE J. Biomed. Health Inform.*, vol. 19, no. 5, pp. 1549–1556, Sep. 2015.

[31] Y. Yao *et al.*, "Mitigation of instrument-dependent variability in ballistocardiogram morphology: Case study on force plate and customized weighing scale," *IEEE J. Biomed. Health Inform.*, vol. 24, no. 1, pp. 69–78, Jan. 2020.

[32] Y. Yao, C. Bruser, U. Pietrzyk, S. Leonhardt, S. van Waasen, and M. Schiek, "Model-based verification of a non-linear separation scheme for ballistocardiography," *IEEE J. Biomed. Health Inform.*, vol. 18, no. 1, pp. 174–182, Jan. 2014.

[33] S. T. Choe and W. D. Cho, "Simplified real-time heartbeat detection in ballistocardiography using a dispersion-maximum method," *Biomed. Res.*, vol. 28, no. 9, pp. 3974–3985, 2017.

[34] S. Hermann, L. Lombardo, G. Campobello, M. Burke, and N. Donato, "A ballistocardiogram acquisition system for respiration and heart rate monitoring," in *Proc. IEEE Int. Instrum. Meas. Technol. Conf. (I2MTC)*, May 2018, pp. 1–5. [Online]. Available: https://ieeexplore.ieee.org/document/8409750/

[35] C. Bruser, J. Diesel, M. D. H. Zink, S. Winter, P. Schauerte, and S. Leonhardt, "Automatic detection of atrial fibrillation in cardiac vibration signals," *IEEE J. Biomed. Health Inform.*, vol. 17, no. 1, pp. 162–171, Jan. 2013.

[36] J. Paalasmaa, H. Toivonen, and M. Partinen, "Adaptive heartbeat modeling for Beat-to-Beat heart rate measurement in ballistocardiograms," *IEEE J. Biomed. Health Inform.*, vol. 19, no. 6, pp. 1945–1952, Nov. 2015.

[37] S. Nurmi, T. Saaresranta, T. Koivisto, U. Meriheinä, and L. Palva, "Validation of an accelerometer based BCG method for sleep analysis," D4 Julkaistu kehittämis- tai tutkimusraportti tai -selvitys, Aalto Univ., Espoo, Finland, Tech. Rep., 2016, pp. 1–16. [Online]. Available: http://urn.fi/URN:ISBN:978-952-60-6842-8

[38] U. Meriheinä, "BCG measurements in beds," Murata Electron., Nagaokakyo, Japan, Tech. Rep., 2019. [Online]. Available: https://bit.ly/2PAhXVA

[39] J. Pan and W. J. Tompkins, "A real-time QRS detection algorithm," *IEEE Trans. Biomed. Eng.*, vol. BME-32, no. 3, pp. 230–236, Mar. 1985.

[40] C. Alvarado-Serrano, P. S. Luna-Lozano, and R. Pallàs-Areny, "An algorithm for beat-to-beat heart rate detection from the BCG based on the continuous spline wavelet transform," *Biomed. Signal Process. Control*, vol. 27, pp. 96–102, May 2016.

Niccolò Mora graduated *(summa cum laude)* in electronic engineering from the University of Parma, Parma, Italy, in 2011. He received the Ph.D. degree (Doctor Europaeus) in information technologies from the University of Parma.

He is currently an Associate Researcher with the Engineering and Architecture Department, University of Parma. His research activity is partly supported and framed within the Ambient Assisted Living (AAL) Joint Programme and the Horizon2020 Programme. His research interests include from Internet-of-Things (IoT)-enabled sensors development (hardware and software) to biosignal processing, with a particular focus on continuous monitoring of vital signs and daily-life human behavioral patterns.

Federico Cocconcelli received the M.Sc. degrees *(summa cum laude)* in electronic engineering from the University of Parma, Italy, in 2015 and 2018, respectively, where he is currently pursuing the Ph.D. degree in information technologies under the supervision Prof. Paolo Ciampolini.

His current research interests include cardiomechanical signals, noninvasive technologies for physiological parameters monitoring, sensors for smart living environments, and signal processing techniques.

Guido Matrella (Member, IEEE) graduated in electronic engineering from the University of Parma, Parma, Italy, in 1999. He received the Ph.D. degree in information technology from the University of Parma in 2003.

Since 2007, he has been a Researcher Assistant with the University of Parma. His scientific work is mainly based on the design of digital systems using HDL descriptions for integrated circuits and field-programmable gate array (FPGAs). In the latest years, his main research activities are framed in the assistive technology field and, in particular, in the use of networks of smart sensors to elderly home behavior monitoring. Within this field, often called Ambient/Active Assisted Living (AAL), he participated in several European projects in the framework of the AAL Joint Programme and Horizon2020.

Paolo Ciampolini graduated *(summa cum laude)* in electronic engineering, Bologna, Italy, in 1983. He received the Ph.D. degree in electronics and computer sciences from the University of Bologna, Bologna, Italy, in 1989.

Since 2001, he has been a Full Professor with the University of Parma, Parma, Italy, where he is in charge of electronics fundamentals and digital design courses. From 2001 to 2008, he was the Chairman of the Board of Electronics at the Engineering Faculty. He is currently serving as a technical/scientific coordinator of two projects funded in the framework of Ambient Assisted Living (AAL) Joint Programme. His research activities include physical and numerical modeling of semiconductor devices, design and optimization of solid-state radiation sensors, digital circuit design, and assistive technology devices.